ACADEMIC PRESS

Available online at www.sciencedirect.com
SCIENCE DIRECT®

Journal of Solid State Chemistry 171 (2003) 84–89

JOURNAL OF SOLID STATE CHEMISTRY

http://elsevier.com/locate/jssc

Charge and orbital order in rare-earth and Bi manganites: a comparison

J.L. García-Munoz,[a,*] C. Frontera,[a] M.A.G. Aranda,[b] C. Ritter,[c] A. Llobet,[a,d] M. Respaud,[e] M. Goiran,[f] H. Rakoto,[f] O. Masson,[g] J. Vanacken,[h] and J.M. Broto[e]

[a] *Institut de Ciència de Materials de Barcelona, CSIC, Campus Universitari de Bellaterra, E-08193 Bellaterra, Spain*
[b] *Universidad de Málaga, 29071 Málaga, Spain*
[c] *Institut Laue-Langevin, 38042 Grenoble Cedex, France*
[d] *Lab. Louis Néel-CNRS, 38042-BP166 Grenoble Cedex 9, France*
[e] *Laboratoire de la Physique de la Matière Condensée, INSA, 135 avenue de Rangueil, F-31077 Toulouse Cedex 4, France*
[f] *Laboratoire National des Champs Magnétiques Pulsés, 143 avenue de Rangueil, BP4245, F-31432 Toulouse Cedex 4, France*
[g] *European Synchrotron Radiation Facility, BP 220, 38043 Grenoble Cedex, France*
[h] *Laboratorium voor Vaste Stof-fysica en Magnetisme, K.U.Leuven, Celestijnenlaan 200 D, B-3001 Heverlee, Belgium*

Received 11 July 2002; received in revised form 1 September 2002; accepted 13 November 2002

Abstract

A comparative investigation of the charge modulation tendencies in R–M–MnO_3 and Bi–Sr–MnO_3 manganites reveals remarkable differences in these series of materials. By means of magnetic, magnetotransport, synchrotron X-ray and neutron diffraction, as well as pulsed high magnetic fields data, we compare the systematic electronic and magnetic properties of several rare-earth-based manganites and bismuth-based Sr manganites. The differences between these types of systems are rationalized in terms of the role that the different electronic structure of bismuth and rare earth plays in these materials.

1. Introduction

Charge ordering (CO) is a fascinating phenomenon in metal oxides with important implications in the 'colossal' magnetoresistance (CMR) of manganese perovskites and in the high-temperature superconductivity of copper oxides. The discovery of CMR, in $R_{1-x}M_xMnO_3$ manganites (R = trivalent lanthanide, M = Ca, Sr, Ba) has led to an explosion of interest in the tendency displayed by many of these manganites to form nanoscopic inhomogeneous states: electronic phase separation and CO phenomena [1–4]. Although the ionic picture [4,5] describes the CO as a real space ordering of the e_g electrons, a more realistic scenario for the CO state in manganites emerges from recent studies [6], which have observed ordered Zener polarons (ZP). In this scenario, each e_g electron is shared by a Mn–O–Mn trio (with quite opened Mn–O–Mn bond angle) instead of a single Mn ion [6]. This sharing is responsible for the ferromagnetic coupling (double-exchange) of the two Mn atoms involved and implies that, in fact, Mn in Zener polarons presents mixed valence.

The stability of CO is determined by the Coulomb repulsion between charges and the elastic energy from the lattice deformations that accommodate the associated orbital ordering. It is known that in many compounds R^{3+} ions and Bi^{3+} ions play the same role. Sometimes, however, this is not so. In this paper we present a comparative investigation of the charge modulation, electronic and magnetic transitions in $R_{1-x}M_xMnO_3$ and $Bi_{1-x}Sr_xMnO_3$ manganites. We mainly focus, although not exclusively, on $x = 1/2$ materials, for which real space charge/ZP-ordering is especially remarkable. Marked differences are found when comparing the physical properties of rare earth and Bi oxides. They can be ascribed to the highly polarizable $6s^2$ lone pair of Bi, which contrary to Bi–Ca–MnO_3 systems plays an active role in Bi–Sr–MnO_3 family.

*Corresponding author. Fax: +34-93-5805729.
E-mail address: garcia.munoz@icmab.es (J.L. García-Munoz).

0022-4596/03/$ - see front matter
doi:10.1016/S0022-4596(02)00192-5

2. Experimental

Polycrystalline R–(Ca,Sr)–MnO_3 and Bi–Sr–MnO_3 ceramics were prepared as black powders by standard solid-state synthesis in air. After some intermediate treatments, the final annealing temperatures were between 1150°C and 1450°C, depending on the compound. Neutron powder diffraction (NPD) patterns were collected at ILL (Grenoble, France) in the temperature interval $1.5 < T < 700$ K. Several diffractometers and wavelengths were used, D2b ($\lambda = 1.594$ Å), D20 ($\lambda = 2.42$ Å) and D1b ($\lambda = 2.52$ Å). Synchrotron powder X-ray diffraction (SXRPD) patterns were collected on BM16 ($\lambda = 0.4424$ Å) diffractometer of ESRF (Grenoble, France) between 170 and 700 K. Structural and magnetic parameters were refined by the Rietveld method using the program FULLPROF [7]. Susceptibility was measured over the range $5 < T < 800$ K. Magnetotransport characterization was performed by the four-probe method, using a commercial PPMS system (Quantum Design) in the temperature range $5 < T < 350$ K. High-magnetic-field studies were performed at the facilities of the SNCMP in Toulouse (France), between 4.2 and 300 K. Using the discharge of a bank capacitor in the coil, pulsed fields up to 50 T (35 T) are obtained with a duration time of 0.6 s (1.6 s). Magnetic field magnetization measurements up to 50 T were also performed in the LVSM in Leuven (Belgium) (pulse duration of 20 ms).

3. Results

3.1. Magnetic, magnetotransport and diffraction measurements

The resistivity of the Sr-doped $R_{0.5}Sr_{0.5}MnO_3$ samples (R = Pr, Nd) and $Bi_{0.5}Sr_{0.5}MnO_3$ at zero field is shown in Fig. 1 below room temperature (RT). The resistivity corresponding to Ca-doped and more distorted $Nd_{0.5}Ca_{0.5}MnO_3$ sample is also shown for comparison. The jump in the resistivity in the rare-earth perovskites contrasts with the absence of resistive transitions in the Bi compound below RT. Fig. 2 shows the temperature dependence of the inverse susceptibility of $x = 1/4$, 1/2 and 2/3 Bi–Sr samples in the temperature range 300–700 K. A clear anomaly can be observed, which besides changes in the Curie temperature, is accompanied by a sudden change in the slope due to the formation of ordered ZPs below the transition. The effective paramagnetic moment changes from $\mu_{eff} = 4.5(1)\mu_B (4.68(4)\mu_B)$ above the transition to $\mu_{eff} = 6.8(4)\mu_B (5.26(2)\mu_B)$ below the transition in $Bi_{0.50}Sr_{0.50}MnO_3$ ($Bi_{0.75}Sr_{0.25}MnO_3$). Moreover, below the transition, NPD and SXRPD data confirm the formation of small superlattice peaks originating from the larger unit cell necessary to describe the structural modulation induced by CO. Fig. 3 shows the evolution in temperature of the integrated intensity corresponding to one of the most intense superstructure peaks for $Nd_{0.5}Ca_{0.5}MnO_3$ (from NPD) and $Bi_{0.5}Sr_{0.5}MnO_3$ (from

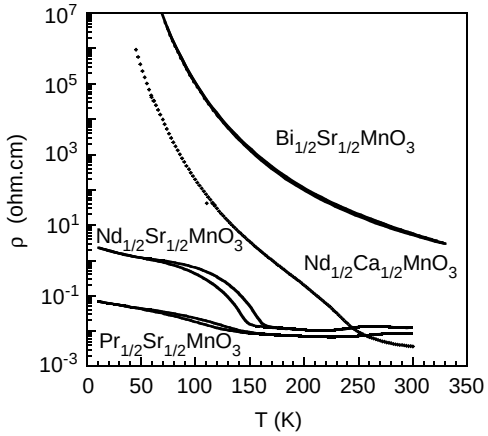

Fig. 1. Comparison of the electrical resistivity in zero field of several $R_{0.5}A_{0.5}MnO_3$ compounds and $Bi_{0.5}Sr_{0.5}MnO_3$.

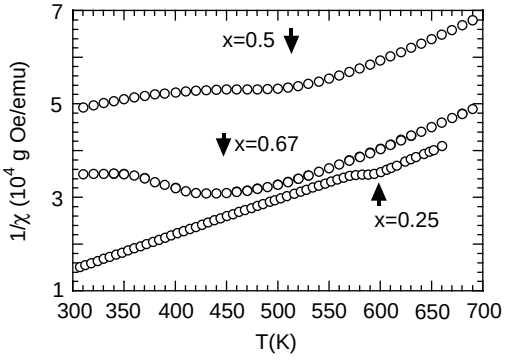

Fig. 2. Inverse susceptibility showing the CO transition in $Bi_{1-x}Sr_xMnO_3$ oxides ($H = 1$ T, curves have been shifted for the sake of clarity).

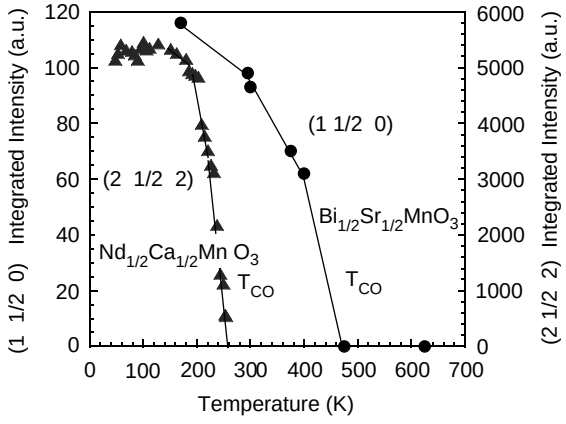

Fig. 3. Integrated intensity of two superlattice peaks as a function of temperature: (1 1/2 0) for $Bi_{1/2}Sr_{1/2}MnO_3$ (from SXRPD), and (2 1/2 2) for $Nd_{1/2}Ca_{1/2}MnO_3$ (from neutron data).

SXRPD). The corresponding indexes are shown in the figure. All the peaks associated with the structural modulation can be indexed by doubling the cell of the average *Pbnm* structure along *b*. The presence of these $\mathbf{k} = (0\frac{1}{2}0)$ superstructure peaks and the *CE*-type magnetic structure observed for the modulated phase (as shown in the left column of Fig. 4 for $Nd_{0.5}Ca_{0.5}MnO_3$ and $Bi_{0.5}Sr_{0.5}MnO_3$) confirm that in all cases the transition is of CO. The lattice parameter evolution with temperature for the average CO cell is shown for $Nd_{0.5}Ca_{0.5}MnO_3$ and $Bi_{0.5}Sr_{0.5}MnO_3$ in Fig. 5(a). The figure illustrates the effects below T_{CO} of the ordered stabilization of FM Mn–Mn pairs. A static component of a cooperative Jahn–Teller distortion appears in both the rare-earth and Bi compounds due to selective orbital ordering occupancy in the *ab* plane.

In Fig. 6 we have gathered the transition temperatures (charge and/or orbital order) in Ca and Sr half-doped manganites, and they are shown as a function of the average $\langle$Mn–O–Mn$\rangle$ distortion determined from neutron diffraction data [8]. Although Bi^{3+} and La^{3+} have very similar ionic radii in many oxides, replacement of La by Bi in this case leads to an increase of the average Mn–O–Mn distortion. The average bonding angle $\langle\theta\rangle = \langle$Mn–O–Mn$\rangle$ is $\approx 5^\circ$ more bent for Bi than for La in $R_{0.5}Sr_{0.5}MnO_3$ series (see Table 1). But $\langle\theta\rangle$ for $Nd_{0.5}Sr_{0.5}MnO_3$ is $\approx 1^\circ$ more bent than for Bi. However, $T_{CO}(Bi_{0.5}Sr_{0.5})$ is more than 350 K higher than $T_{CO}(Nd_{0.5}Sr_{0.5})$. A behavior that falls out of the classical bandwidth tuning approach for the evolution of T_{CO} as a function of the average tilting of the octahedra in the $R_{1/2}M_{1/2}MnO_3$ series [9,10]. The extraordinarily high CO transition temperature in $Bi_{1/2}Sr_{1/2}MnO_3$ (525 K) has no precedent in *R*–Mn–O manganites, and cannot be justified by simply considering the average buckling of the Mn–O–Mn bonds.

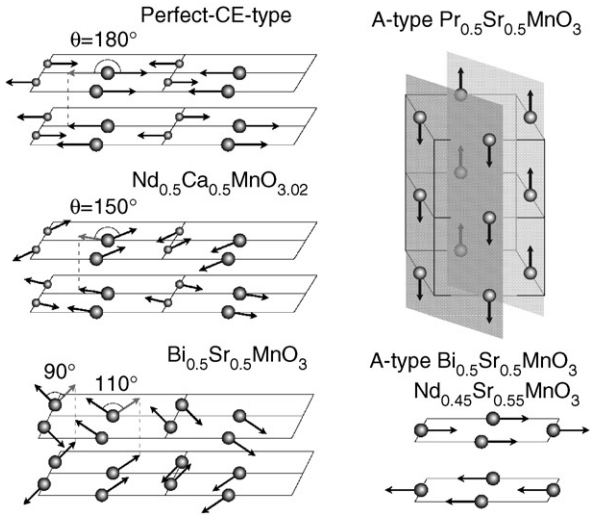

Fig. 4. Comparison of the magnetic structures observed in several $R_{1/2}A_{1/2}MnO_3$ phases.

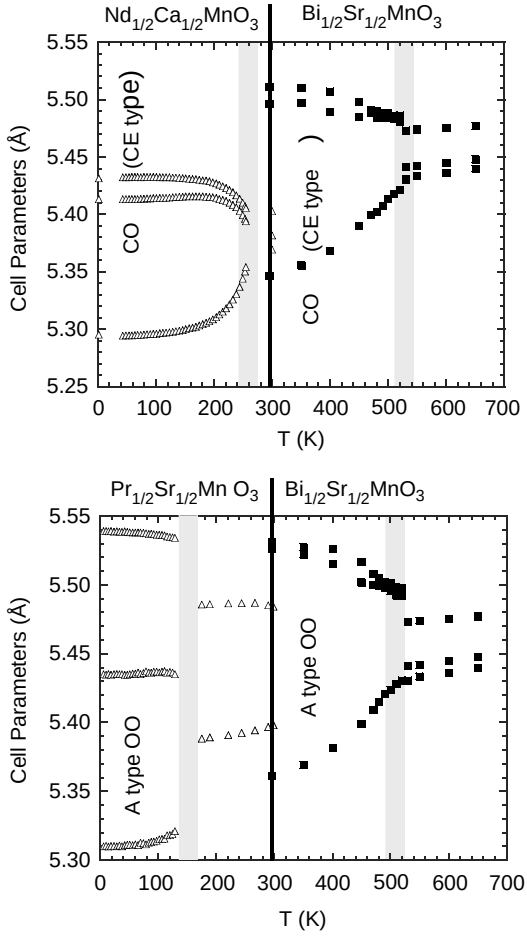

Fig. 5. (a) Comparison of the temperature evolution of the lattice parameters of the *CE*-type $Nd_{1/2}Ca_{1/2}MnO_3$ (open) and $Bi_{1/2}Sr_{1/2}MnO_3$ (filled symbols) phases. (b) Temperature evolution of the lattice parameters of the *A*-type phases of $Pr_{1/2}Sr_{1/2}MnO_3$ and $Bi_{1/2}Sr_{1/2}MnO_3$ compounds.

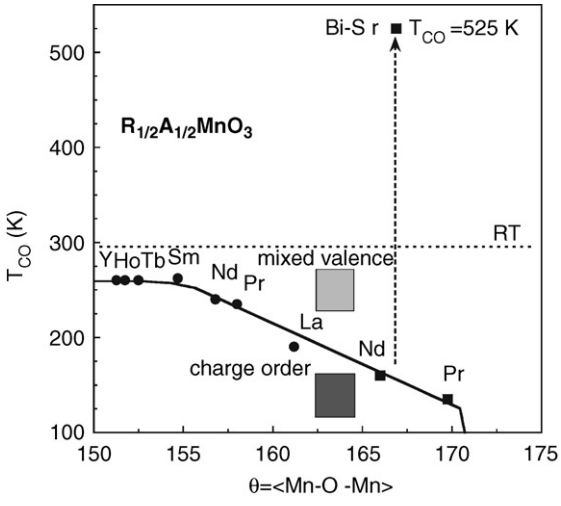

Fig. 6. Dependence of the ordering temperature T_{CO} for $R_{1/2}A_{1/2}MnO_3$ (A = Ca, solid circles, and Sr, solid squares) on the average Mn–O–Mn angular distortion. Note the saturation below RT decreasing the *R* size.

Table 1
Comparative interatomic distances and angles of $R_{1/2}Sr_{1/2}MnO_3$ oxides at RT

Sample	θ_1 (deg)[a]	θ_2 (deg)[a]	$\langle\theta\rangle$ (deg)	d_1 (Å)[a]	d_2 (Å)[a]	$\langle d_{Mn-O}\rangle$
$Nd_{1/2}Sr_{1/2}$	162.4(4)	167.8(3)	166.0(3)	1.931(1)	1.939(1)	1.936(1)
$Bi_{1/2}Sr_{1/2}$	164.7(1)	168.0(7)	166.9(5)	1.910(1)	1.963(4)	1.945(2)
$Pr_{1/2}Sr_{1/2}$	180	164.3(2)	170.1(1)	1.947(1)	1.928(1)	1.934(1)
$La_{1/2}Sr_{1/2}$	180	168.6(2)	172.4(1)	1.9338(2)	1.9376(6)	1.936(1)

[a] θ_1, θ_2, d_1, and d_2 stand for $\theta_{Mn-O1-Mn}$, $\theta_{Mn-O2-Mn}$, $\langle d_{Mn-O1}\rangle$ and $\langle d_{Mn-O2}\rangle$, respectively.

As shown by the resistivity measurements, there is a strong decrease of the mobility of e_g electrons when Bi substitutes a big rare-earth in Sr-doped manganites. The resistivities of $Bi_{0.5}Sr_{0.5}MnO_3$ measured (heating) at $\mu_0 H = 0$ and 5 T are depicted in Fig. 7. It is apparent that this compound does not present any significant magnetoresistance for an applied field of 5 T. For comparison, we have also plotted in this figure the corresponding resistivity of polycrystalline $Pr_{0.5}Sr_{0.5}MnO_3$, which shows the recovery of the ferromagnetic metallic state under such a moderate field. At this point we recall that the carrier mobility is strongly reduced in very distorted manganites such as $Y_{0.5}Ca_{0.5}MnO_3$, $Ho_{0.5}Ca_{0.5}MnO_3$ or $Tb_{0.5}Ca_{0.5}MnO_3$. Nevertheless, in spite of having a reduced one-electron effective bandwidth and a high degree of strain in the structure, $T_{CO} < 300$ K in all these compounds (see Fig. 6). The material has always to be cooled for stabilizing the CO phase. This is in great contrast with $Bi_{0.5}Sr_{0.5}MnO_3$.

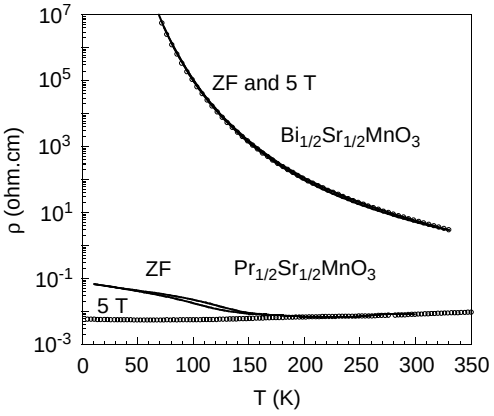

Fig. 7. Comparison of the electrical resistivity in zero field and 5 T of $Pr_{1/2}Sr_{1/2}MnO_3$ and $Bi_{1/2}Sr_{1/2}MnO_3$.

3.2. High magnetic field study

The existence of remarkable differences between $R_{0.5}(Ca,Sr)_{0.5}MnO_3$ and $Bi_{0.5}Sr_{0.5}MnO_3$ oxides has been also confirmed by studying the stability of the CO/OO phases in high magnetic fields. Charge and orbital ordered states can be disrupted under application of external fields. In the magnetic-field-melting mechanism the induced polarization of the electronic spins competes with the trapping of the charges and favors their delocalization. Isothermal magnetization measurements, using long pulsed magnetic fields, were done after a zero-field cooling process. The magnetization measurements at 4.2 K of the perovskites with Sm–Ca, Pr–Ca, La–Ca and Bi–Sr are shown in Fig. 8. In the rare-earth manganites the sudden increase in the magnetization is related to the melting of the CO/OO state. The thermodynamic transition field, H_C, is defined as the average of the saturation fields (H_c^+ and H_c^-, for the up and down sweeps). In Fig. 9 we have plotted the evolution of the thermodynamic transition fields (H_c) at 4 K as a function of the ordering temperature T_{CO}. It is apparent that Bi–Sr falls out of the general tendency to smaller transition fields in the half-doped rare-

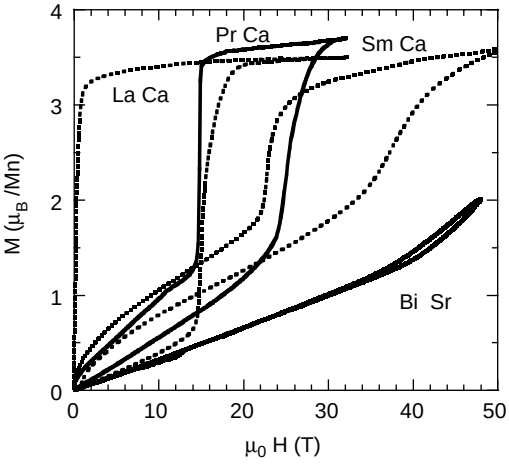

Fig. 8. Magnetization versus field curves of several $R_{1/2}A_{1/2}MnO_3$ compounds measured at 4.2 K.

earth compounds as the R size increase. Notice that an external field of 8 T is enough to melt the CO state of $Nd_{1/2}Sr_{1/2}MnO_3$, whereas the CO state of $Bi_{1/2}Sr_{1/2}MnO_3$ is unaffected by a magnetic field of 40 T. To fully saturate the Mn magnetic moments in the latter ($3.5\mu_B$/Mn), fields higher than 50 T are required. At least 40 T more than in $La_{1/2}Ca_{1/2}MnO_3$. For the sake of comparison, such a field is enough to provoke

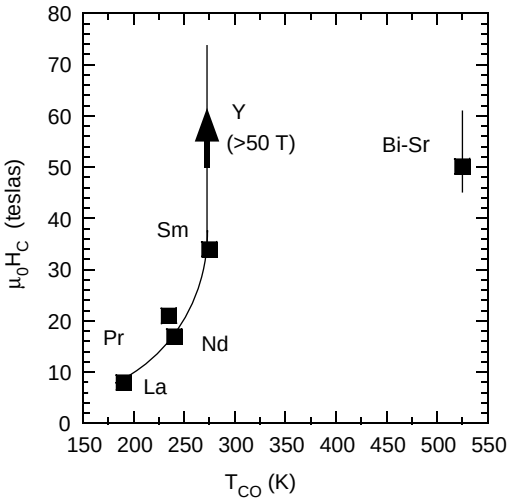

Fig. 9. Relationship between the thermodynamic critical field H_c for charge melting and the ordering temperature T_{CO} for several $R_{1/2}A_{1/2}MnO_3$ oxides.

the melting of the CO state in the very distorted $Sm_{0.5}Ca_{0.5}MnO_3$ oxide.

4. Discussions and conclusions

There are several reports dealing with the evolution of the tilt system increasing the size of the A cations [9,10]. At RT all of the $R_{1/2}Ca_{1/2}MnO_3$ compounds have *Pbnm* (or *Pnma*) symmetry [9–11]. At low temperatures, in the manganites with narrow bandwidth the commensurate $\mathbf{k} = (0\frac{1}{2}0)$ modulation associated to the *CE*-type charge ordered state persists for x values even well below the $x = 1/2$ doping. For instance, the structural modulation is $\mathbf{k} = (0\frac{1}{2}0)$ in $Pr_{1-x}Ca_xMnO_3$ within the interval $1/3 < x < 1/2$, where the so-called pseudo-*CE*-type magnetic structure is found. On another hand, for an off-stoichiometry corresponding to values of the Mn^{4+}:Mn^{3+} ratio larger than one (over-doped samples) [12,13], the structural modulation follows the electron concentration $\mathbf{k} = (0\ \ (1-x)\ \ 0)$. Microscopically, this occurs as the result of the alternation of different types of commensurate structures [12,14].

The scenario in Sr-doped manganites, which present wider e_g bandwidths and more straightened Mn–O–Mn bonds, is rather different. An evolution with R of the tilt system has been observed at RT giving more anisotropic oxides [10]. At low temperatures, *CE*-type CO state occurs in a very narrow compositional range around $x = 0.5$ in Sr-doped manganites with R-sizes between Nd and Pr. To be emphasized is that, at variance with $Bi_{0.5}Sr_{0.5}MnO_3$, pseudo-*CE*-type magnetic ordering has not been previously observed in Sr-doped manganites around $x \sim 1/2$. Instead, the FM metallic ($x \leqslant \sim 0.5$) and AFM metallic ($x \geqslant \sim 0.5$) *A*-type ordered phases [15] (for $R[\mathrm{Nd}] < R < R[\mathrm{Pr}]$) compete with *CE*-type CO. Finally, for $R > R[\mathrm{Pr}]$, *CE*-type CO structure is substituted by *A*-type (charge disordered) phase. Moreover, the *A*-type *CE*-type competition occurs for a quite small x-range, *R*–Sr manganites having a Mn^{4+}:Mn^{3+} ratio significantly higher than 1 stabilize an *A*-type phase. These general features contrasts with the behavior of Bi–Sr compounds.

Above T_{CO}, diffraction data for our $Bi_{0.5}Sr_{0.5}MnO_3$ sample was consistent with a single *Pbnm* phase. Decreasing temperature the sample actually splits into two macroscopic phases with slightly different lattice parameters when cooled below T_{CO}. Fig. 5 illustrates the evolution of the refined lattice parameters for, hereafter, *CE*-type Bi–Sr [55 wt%, modulation vector $\mathbf{k} = (0\frac{1}{2}0)$] and *A*-type Bi–Sr [45 wt%, modulation vector $\mathbf{k} = (000)$] phases. As a result of the aforementioned competition between *A* and *CE*-phases, macroscopic phase segregation is commonly observed in samples with even very small compositional fluctuations these two phases (*CE*- and *A*-type) have very similar energies [9]. The corresponding magnetic structures (pseudo-*CE*- and *A*-type) are shown in Fig. 4. For both magnetic phases we have observed $T_N \approx 150$ K.

Next, we want to focus on the comparison of the *A*-type phases of rare-earth and Bi manganites doped with Sr. In fact, our results indicate that they are quite different. First, orbital and magnetic order occur simultaneously in the *A* phase with rare-earths ($T_N = T_{OO}$). For Bi, the evolution of the lattice parameters in Fig. 5(b) tells us that $T_{OO} \approx 525$ K, while $T_N \approx 150$ K. The rare-earth *A* phases are 2D metallic antiferromagnets [16,17], characterized by a planar x^2–y^2-type orbital ordering that yields highly conductive 2D bands. The resistivity is metallic-like above T_{OO} and remains moderately low even below this temperature [16]. On the other hand, Figs. 1 and 7 confirm that the resistivity of the Bi *A* phase is several orders of magnitude higher (the proportion of the *A*-type phase in the sample of Fig 1, 45 wt%, warrants that it percolates the system). Furthermore, Fig. 8 confirms that the orbital-order stability under field in Bi *A* phase is very high. This is in contrast with the fragility of the rare-earth case. Related to this, the different magneto-resistive response of both *A*-type phases is very apparent in Fig. 7. Thus, there is strong charge localization in the Bi–Sr *A* phase which contrasts with the 2D metallic state in the *R*–Sr case. Consequently, an important question is whether, in this *A*-type phase, e_g electrons are randomly distributed (disordered) on the Mn^{4+} sites or do they form an ordered structure. Does exists Zener polaron ordering also in this phase? It is clear that the double-exchange interaction is not the main responsible for the ferromagnetic planes in the Bi–Sr *A* phase, despite it is the most probable scenario with rare earths. For Bi, the *A*-type magnetic order can be easily

explained if e_g electrons order in the planes, confined in $d_{x^2-y^2}$ orbitals, forming a check-board structure. On the contrary, a random localization of e_g electrons (absence of CO) would induce frustration in the magnetic interactions. In consistence with present data, the proposed CO/OO does not imply supercell periodicity or superlattice peaks. The search of the associated breathing-type distortion requires additional works that are in course.

The tendency in R–Ca manganites to real space charge or polaron ordering is especially remarkable for $x = 1/2$ doping. Changing the doping level to lower (or higher) values (unbalance of electrons and holes) has been found to decrease T_{CO} or even suppress CO as happens in R–Sr compounds. In particular, the excess electrons weaken the strength of the CO state: T_{CO} decreases from ~ 240 K for $x = 0.5$ to ~ 200 K for $x = 0.3$ in the $Pr_{1-x}Ca_xMnO_3$ series [18] and CO disappears for $La_{0.55}Ca_{0.45}MnO_3$, while $La_{0.5}Ca_{0.5}MnO_3$ presents $T_{CO} \sim 225$ K [19]. The higher stability of CO in half-doped samples is usually attributed to the fact that the Coulomb energy gain due to CO and the strain energy gain due to OO are maximal when Mn^{3+}/Mn^{4+} ratio is 1. This is not so in (Bi,Sr)MnO_3 compounds. As suggested by Fig. 2 the charge-ordered phase of $Bi_{0.75}Sr_{0.25}MnO_3$ presents a transition temperature $T_{CO} = 600$ K (see also Ref. [20]), well above the ordering temperature in half-doped $Bi_{0.50}Sr_{0.50}MnO_3$ ($T_{CO} = 525$ K). Hence, in underdoped $Bi_{0.75}Sr_{0.25}MnO_3$, an off-stoichiometry corresponding to a Mn^{3+}/Mn^{4+} ratio of 3 increases T_{CO} by ~ 75 K with respect to half-doping. This is against the general tendency displayed by rare-earth-based manganites. This unusual behavior must be attributed to the increase in the concentration of bismuth, and it is a confirmation of the key role of Bi^{3+} ions in CO phenomena displayed by $Bi_{1-x}Sr_xMnO_3$ series.

The possibility that Bi and Sr form some kind of ordering was examined and has to be ruled out in these oxides. According to the structural data given in Refs. [8,21] the present results suggest that the $6s^2$ lone pair of Bi^{3+} is weakly screened in (Bi,Sr)MnO_3 compounds. An orientation of the $6s^2$ lone pair toward a surrounding anion (O^{2-}) can produce a local distortion or even a hybridization between 6s-Bi-orbitals and 2p-O-orbitals [8,21]. As a result the movement of e_g electrons through the Mn–O–Mn bridges can be severely reduced and charge order tendency strongly favored.

Acknowledgments

Financial support by the CICyT ((MAT97-0699), MEC (PB97-1175) projects and funding the CRG-D1B line), el Departament d'Universitats, Recerca i Societat de la Informació de la Generalitat de Catalunya (GRQ95-8029, PICS2001-22). The provision of beam time at ILL (neutrons) and ESRF (synchrotron X-rays) facilities is acknowledged. The SNCMP INSA (Toulouse, France) and LVSM (Leuven, Belgium) laboratories are acknowledged for making available their experimental facilities.

References

[1] E.O. Wollan, W.C. Koehler, Phys. Rev. 100 (1955) 545.
[2] A. Moreo, S. Yunoki, E. Dagotto, Science 283 (1999) 2034.
[3] S. Mori, C.H. Chen, S.-W. Cheong, Nature 392 (1998) 473.
[4] J.B. Goodenough, Phys. Rev. 100 (1955) 564.
[5] P.G. Radaelli, D.E. Cox, M. Marezio, S-W. Cheong, Phys. Rev. B 55 (1997) 3015.
[6] A. Daoud-Aladine, et al., Phys. Rev. Lett. 89 (2002) (cond-mat/0111267) (2002) 097205.
[7] J. Rodríguez-Carvajal, Physica (Amsterdam) 192B (1993) 55.
[8] J.L. García-Muñoz, C. Frontera, M.A. García-Aranda, A. Llobet, C. Ritter, Phys. Rev. B 63 (2001) 064415.
[9] C.N.R. Rao, A. Arulraj, P.N. Santosh, A.K. Cheetham, Chem. Mater. 10 (1998) 2714.
[10] P.M. Woodward, D.E. Cox, T. Vogt, C.N.R. Rao, A.K. Cheetham, Chem. Mater. 11 (1999) 3528.
[11] M. Respaud, et al., Phys. Rev. B 61 (2000) 9014.
[12] C. Frontera, J.L. García-Muñoz, A. Llobet, C. Ritter, J.A. Alonso, J. Rodríguez-Cavajal, Phys. Rev. B 62 (2000) 3002.
[13] W.-H. Li, S.Y. Wu, K.C. Lee, J.W. Lynn, R.S. Liu, J.B. Wu, C.Y. Huang, J. Appl. Phys. 85 (1999) 5588.
[14] A. Barnabé, M. Hervieu, C. Martin, A. Maignan, B. Raveau, J. Appl. Phys. 84 (1998) 5506.
[15] R. Kajimoto, H. Yoshizawa, H. Kawano, H. Kuwuhara, Y. Tokura, K. Ohoyama, M. Ohashi, Phys. Rev. B 60 (1999) 9506.
[16] F. Damay, C. Martin, M. Hervieu, A. Maignan, B. Raveau, G. Andre, F. Bouree, J. Magn. Magn. Mater. 184 (1998) 71.
[17] A. Llobet, J.L. García-Muñoz, C. Frontera, C. Ritter, Phys. Rev. B 60 (1999) R9889.
[18] Z. Jirák, S. Krupicka, Z. Simsa, M. Dlouha, S. Vratislav, J. Magn. Magn. Mater. 53 (1985) 153.
[19] J. Alonso, et al., Phys. Rev. B 64 (2001) 172410.
[20] C. Frontera, et al., Solid State Comm. 125 (2003) 277.
[21] C. Frontera, J.L. García-Muñoz, M.A.G. Aranda, A. Llobet, C. Ritter, M. Respaud, J. Vanacken, Phys. Rev. B 64 (2001) 054401.